Earth and Planetary Science Letters 402 (2014) 127–137

Contents lists available at ScienceDirect

Earth and Planetary Science Letters

www.elsevier.com/locate/epsl

3-D structure of the Rio Grande Rift from 1-D constrained joint inversion of receiver functions and surface wave dispersion

Anibal Sosa [a,*], Lennox Thompson [b], Aaron A. Velasco [b], Rodrigo Romero [c], Robert B. Herrmann [d]

[a] Universidad Icesi, Cali, Colombia
[b] Department of Geological Sciences, University of Texas at El Paso, El Paso, 79968-0555, United States
[c] Department of Computer Science, University of Texas at El Paso, El Paso, 79968-0555, United States
[d] Department of Earth & Atmospheric Sciences, Saint Louis University, St. Louis, MO 63108, United States

ARTICLE INFO

Article history:
Accepted 2 June 2014
Available online 23 June 2014
Editor: P. Shearer

Keywords:
Rio Grande Rift
computational geosciences
Jemez lineament

ABSTRACT

The Southern terminus of the Rio Grande Rift region has been poorly defined in the geologic record, with few seismic studies that provide information on the deeper Rift structure. In consequence, important questions related to tectonic and lithospheric activity of the Rio Grande Rift remain unresolved. To address some of these geological questions, we collect and analyze seismic data from 147 EarthScope Transportable Array (USArray) and other seismic stations in the region, to develop a 3-D crust and upper mantle velocity model. We apply a constrained optimization approach for joint inversion of surface wave and receiver functions using seismic *S* wave velocities as a model parameter. In particular, we compute receiver functions stacks based on ray parameter, and invert them jointly with collected surface wave group velocity dispersion observations. The inversions estimate 1-D seismic *S*-wave velocity profiles to 300 km depth, which are then interpolated to a 3-D velocity model using a Bayesian kriging scheme. Our 3-D models show a thin lower velocity crust anomaly along the southeastern Rio Grande Rift, a persistent low velocity anomaly underneath the Colorado Plateau and Basin and Range province, and another one at depth beneath the Jemez lineament, and the southern RGR.

1. Introduction

Bounded by the Basin and Range province and the Colorado Plateau to the west and the Great Plains to the East, the Rio Grande Rift (RGR) extends approximately 1000 km from central Colorado to El Paso, Texas (Fig. 1). The RGR has recent volcanism, fault scarps, and seismicity (Fig. 2) and is widening at a modest rate of about 0.5 mm/yr or less (Berglund et al., 2012; Kreemer et al., 2010; Woodward, 1977). Although many studies have focused on the Rift system (e.g., Averill et al., 2007; Gao et al., 2004; Keller et al., 1991; Roy et al., 2005; van Wijk et al., 2008; West et al., 2004a; Wilson et al., 2005a, 2005b), the southern terminus of the RGR remains poorly defined (Keller and Baldridge, 1999) and few seismic studies have provided detailed information on the deeper rift structure (Averill et al., 2007; Gao et al., 2004; Keller et al., 1991).

Studies of the RGR present several possible Earth models and interpretations, which may be due to the diversity of the methodologies implemented and the specific location of the study (Gao et al., 2004; Moucha et al., 2008; van Wijk et al., 2008; West et al., 2004b). For example, Keller (2004) presented a Moho depth map, based on a compilation of previous studies, and showed significant crustal thinning (∼28 km) in the southern RGR. Averill et al. (2007) conducted a controlled source experiment and developed a detailed profile across the southern RGR, showing a crustal thickness of around 32 km. Gao et al. (2004) proposed that small convection cells in the deeper mantle are responsible for recent magmatic and tectonic activity, while Chapin and Cather (1994) propose that rotation of the Colorado Plateau played a role in rift formation.

More recent studies in the region have taken full advantage of data collected by EarthScope's Transportable Array (USArray) to develop models that are derived from a variety of approaches: seismic tomography (Becker, 2012; Bensen et al., 2009; Buehler and Sheare, 2012, 2010; Burdick et al., 2010; Moschetti et al., 2010; O'Driscoll et al., 2011; Pavlis et al., 2012; Sigloch, 2011; Steck et al., 2011; Tian et al., 2011; Xue and Allen, 2010; Yang et al., 2008; Yuan et al., 2011; Yuan and Romanowicz, 2010), receiver functions (Abt et al., 2010; Cao and Levander, 2010; Gilbert, 2012;

* Corresponding author. Tel.: +57 2 555 2334x8195; fax: +57 2 555 1441.
E-mail address: uasosa@icesi.edu.co (A. Sosa).

http://dx.doi.org/10.1016/j.epsl.2014.06.002
0012-821X/

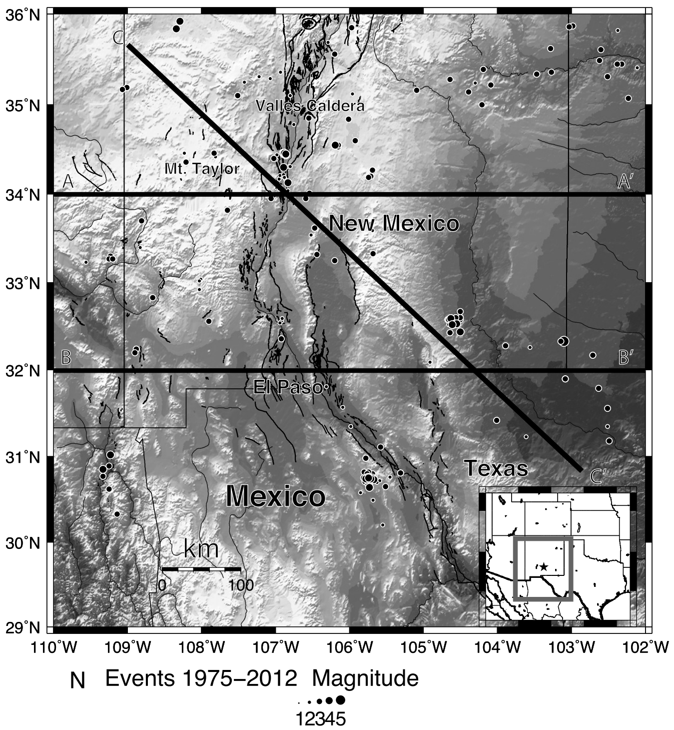

Fig. 1. Topography map of the RGR with all the seismicity, plotted from 1975–2012, represented by black circles and faults illustrated by the light black lines. The small inset map on the lower right hand corner indicates our study area for this research. There are also three profiles outlined by the solid black lines labeled A–A′, B–B′, and C–C′. These profiles cross all major tectonic provinces that lie within the RGR region. All the profiles in this figure were investigated to obtain a better understanding of the crust/upper mantle structure of the entire rift system.

Hansen et al., 2013; Levander and Miller, 2012; Miller and Eaton, 2010; West et al., 2004a; Wilson et al., 2010), joint inversions (Bailey et al., 2012; Lin et al., 2012; Moucha et al., 2008; West et al., 2004b). Many models show the main tectonic regions in North America, but do not necessarily focus on rift formation.

Besides the availability of new data and recent studies on the RGR, important questions about the Rift evolution remain unresolved: 1) is it actively deforming along its southern extent (Berglund et al., 2012; Keller and Baldridge, 1999; Moucha et al., 2008)?; 2) does it propagate southward?; 3) what is the role of mantle convection in the formation of the Rift?; 4) does partial melt and unstable lithosphere composition affect the rift's evolution (Gao et al., 2004; West et al., 2004a; Wilson et al., 2005b)?; and 5) how does it influence the evolution of adjacent areas within the North American Plate (Roy et al., 2005)?

In this paper, we revisit the driving forces that cause RGR formation using high quality available data and applying a robust inversion/imaging method for an integrated analysis of Earth structure that allows us to create three-dimensional (3-D) velocity models. Specifically, we determine the crustal and upper mantle structure of the RGR using the USArray data (http://www.earthscope.org) along with other data sets. We apply a constrained optimization 1-D joint inversion approach (Sosa et al., 2013) using receiver functions for 147 USArray and the LA RISTRA (Colorado Plateau/Rio Grande Rift Seismic Transect Experiment; Gao et al., 2004; West et al., 2004a) stations (Wilson et al., 2005a, 2005b; Thompson et al., submitted for publication), and a high quality surface wave dispersion data set provided (Herrmann et al., 2013), and then interpolate the results to obtain a 3-D shear velocity model of the region. Based on our results, we find little evidence of deep mantle upwelling to drive the rifting of the RGR region.

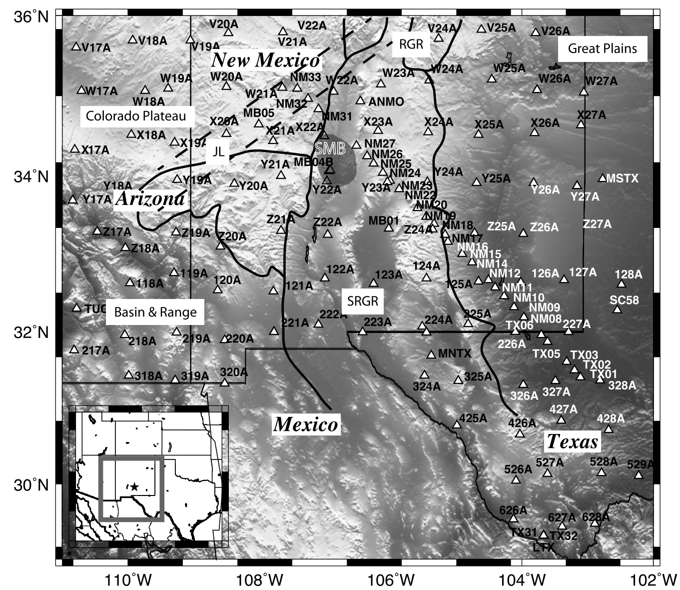

Fig. 2. Regional topography of the New Mexico, Texas, and Mexico border region and approximate tectonic boundaries (Basin and Range, Colorado Plateau, Great Plains, southern Rio Grande Rift (SRGR)) based on Bashir et al. (2011), Keller and Baldridge (1999), Song and Helmberger (2007), Wilson et al. (2005a, 2005b). The white triangles represent the seismic stations from which we used data for this study, including NM stations, ANSS backbone stations (MNTX, ANMO, MSTX), IMS network stations (TX31, TX32), and USArray stations (all other stations).

2. Tectonic setting

The RGR, a major continental rift, that formed in the late Oligocene or early Miocene (Cook et al., 1978) separates the Proterozoic continental lithospheres of the western Great Plains and the Colorado Plateau (Bashir et al., 2011; Keller and Baldridge, 1999; Moucha et al., 2009; Roy et al., 2009; Song and Helmberger, 2007). An initial stage of extension began at 30–20 Ma, with low-angle faulting and crustal doming. The second phase (3–10 Ma) involved 10% extension trending in the E-W direction (Keller et al., 1990; Wilson, 2003). Wilson (2003) hypothesized that this extension resulted from upper mantle asthenosphere upwelling and thermal lithosphere erosion. Extension along the western interior portion of North America stimulated the formation of the RGR, leaving the Colorado Plateau undeformed during this period (e.g., Liu and Gurnis, 2010; Wilson, 2003). Keller and Baldridge (1999) highlight that the southern RGR has experienced more extension than the northern section of the rift, while Kreemer et al. (2010) did not find significant extension across most of the RGR but the southernmost part (∼0.5 mm/yr). Berglund et al. (2012) also show that the extensional deformation is not concentrated in a narrow zone centered on the Rio Grande Rift but rather is distributed broadly from the western edge of the Colorado Plateau well into the western Great Plains.

The Rio Grande rift broadens and changes strike at the US–Mexico border (Fig. 2) and has evidence of volcanism and seismicity. Volcanism was prominent in the rift area during the Pliocene and Quaternary (Cook et al., 1978), and also during the Cenozoic especially along the trend called Jemez lineament to the west of the rift (Gao et al., 2004). It is associated with large negative gradients in lithospheric thickness on both sides of the rift (Levander and Miller, 2012). Although the RGR is not as seismically active as other parts of the North American plate margin, the faults in the region show Quaternary offsets (Collins and Raney, 1994). The RGR does appear to remain more seismically active than the adjacent Basin and Range Province (Machette, 1998) suggesting that the two regions may be responding to extensional processes differ-

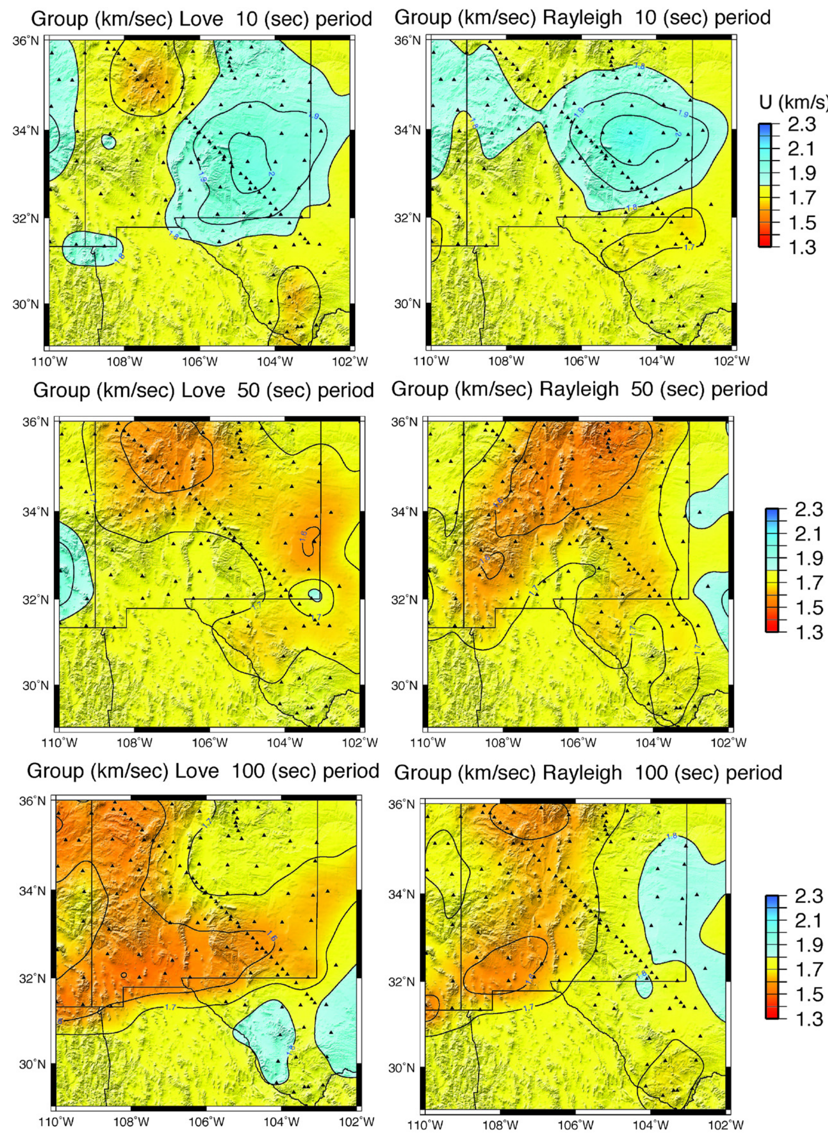

Fig. 3. We show group velocity maps for the RGR region using 3 different periods (10 s, 50 s, and 100 s). The black triangles represent all the seismic stations that we used to plot the group velocity maps for the rift system. From the group velocity maps, we note that we can resolve the different tectonic provinces at different periods, in particular the slow velocities that persist at longer periods within the Basin and Range province.

ently. Additionally, the extension directions during rifting appear to have rotated in a clockwise sense since its inception at ∼30 Ma (Keller et al., 1990 and references therein), but the causes of this rotation remain unknown.

The LA RISTRA passive experiment results have shown that the center of the RGR has a low velocity zone in the upper mantle (Gao et al., 2004; West et al., 2004b; Wilson et al., 2005a), suggesting that there could be melt material or that the crust is thinning beneath the center of the RGR. The zone of crustal thinning widens southward as does the physiographic expression of the rift. In southern New Mexico, the RGR seems to have experienced more deformation from a geophysical perspective, creating the thinnest crust (less than 30 km) with very high heat flow (Keller, 2004). Roy et al. (2005) integrated seismic velocities, gravity and xenolith data, to explore temperature and compositional variations together with partial melt content beneath the eastern Colorado Plateau and RGR. They interpreted the results of that study as a product of modified and/or thinned lithosphere. Furthermore, Roy et al. (2005) argue that the RGR and southeastern Colorado Plateau were underlain by a low-density upper mantle province, which does not trend along upper crustal tectonic boundaries, but correlates with regions of late Tertiary magmatism. Recently, Bailey et al. (2012) jointly inverted seismic data constrained by gravity anomalies concluding that the low velocity mantle beneath the RGR indicates that some removal of the lithosphere has occurred.

3. Receiver functions

A receiver function maps the seismic response of the earth beneath a seismic station to an incoming, teleseismic *P* wave. Deconvolving the vertical component of a teleseismic earthquake seismogram from the radial component (e.g., Langston, 1981) results in a receiver function, which then allows for the identification of converted phases corresponding to strong impedance contrasts (e.g., the crustal–mantle boundary). Since we use teleseismic events that arrive at the stations with near-vertical incidence, receiver functions can also be used for imaging deep structure (Gilbert et al., 2007; Hansen et al., 2013; Kumar et al., 2012; Levander and Miller, 2012; Schmedes et al., 2012). Furthermore, receiver functions can provide valuable information for investigating magma lenses within the crust, determining the Moho depth, other upper-mantle discontinuities (Lodge and Helffrich, 2009), structure and evolution of the crust (Bashir et al., 2011), and rifting extension and magmatism (e.g., Dugda et al., 2005).

For this study, we collect three-component seismic data for 147 stations within the area of latitudes between 29° to 36°N and longitudes between −111° to −102°E (Fig. 1) from the LA RISTRA portable seismic experiment, EarthScope transportable array (USArray), United States Geological Survey ANSS backbone stations, and the International Monitoring System (IMS) network stations in the region (Thompson et al., submitted for publication). The nominal spacing (∼70 km) between USArray stations allows for both lower crustal and upper mantle seismic studies (Schmedes et al., 2012). The LA RISTRA experiment recorded data for a year and a half beginning in August 1999. Thompson et al. (submitted for publication) compared their findings with the EarthScope Automated Receiver Survey (EARS) website results (http://www.seis.sc.edu/ears/), and found inconsistencies that are likely the result of differing quality control parameters and loss of high frequency information (Schmedes et al., 2012; Wilson and Aster, 2005). We utilize the receiver function data set provided by Thompson et al. (submitted for publication), which includes 434 receiver functions stacked in ray parameter bins derived from 1464 teleseismic seismic events with a minimum moment magnitude of 5.5 and occurring from January, 2000 to December, 2009. This data set focuses in the southern Rio Grande Rift, although the area of the imaged region is much larger (Thompson et al., submitted for publication).

4. Surface wave dispersion

In general, surface waves dominate seismograms as the largest amplitude waves from an earthquake and have observed lower frequencies than body waves. Furthermore, surface wave velocities vary depending on the depth sampled by each period, resulting in dispersion. Measuring dispersion of surface waves provides valuable information for studying Earth's crustal and mantle velocity structure (Obrebski et al., 2010; Shearer, 2009; Stein and Wysession, 2009). In particular, Love and Rayleigh wave group dispersion observations generally account for average velocity structure as a function of depth (Julia et al., 2000; Maceira and Ammon, 2009; Shearer, 2009; Stein and Wysession, 2009).

As part of the systematic determination of earthquake moment tensors for North American earthquakes, Saint Louis University measures fundamental mode Love and Rayleigh wave spectral amplitudes and group velocities using a multiple filter analysis from local to regional earthquakes. Tomographic methods are then used to obtain maps of group velocity dispersion for North America with emphasis on the continental United States (Ammon, personal communication; Cho et al., 2007). As of December 2013, there were over 2,020,514 dispersion measurements available for use. Furthermore, the dataset contains dispersion measurements from regional earthquakes, which allows for measurements at shorter periods (less than 15 s) and more sensitivity to shallower Earth structure (upper mantle and crust). We extract the dispersion curves at each station from the tomographic maps (Herrmann et al., 2013) for our analysis of the RGR.

To demonstrate the stability of the measurements, we interpolate the surface wave data for several periods (Fig. 3) using Bayesian kriging (Schultz et al., 1999). Fig. 3 shows group velocity maps for the RGR region using 3 different periods (10 s, 50 s, and 100 s), although we include periods up to 140 s. From the group velocity maps, we distinguish the different tectonic provinces at different periods, in particular the slow velocities that persist at longer periods in the Basin and Range province. To determine how deep the surface wave data can resolve for our joint inversion, we calculate data sensitivity kernels for several stations (Herrmann and Ammon, 2002). Fig. 4 shows the surface waves sensitivity kernels plotted as a function of depth for a suite of periods used in our analysis. From this calculation, we determine that the surface waves resolve to approximately 300 km of depth; thus, we include results from 10–300 km in depth for our 3-D models.

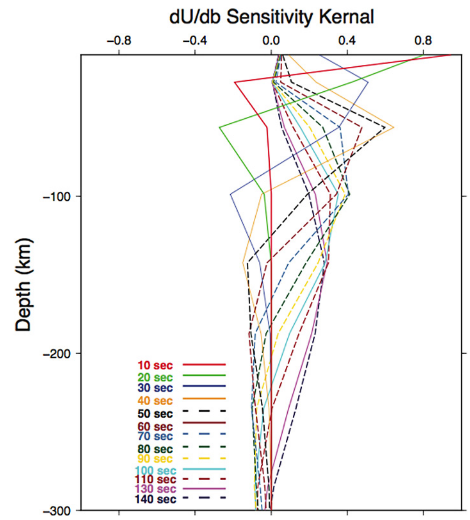

Fig. 4. Sensitivity kernels for surface wave dispersion for four different stations located at each province included in this study. The surface wave's sensitivity kernels are plotted as a function of depth for several periods. Based on the sensitivity kernel plots, we are able to determine what depth we can resolve, which is about 300 km depth.

5. 1-D constrained joint inversion

Joint inversion involves the simultaneous optimization of several objective functions, such as the ℓ_2-norm data misfit. Since the objective function is expected to be less subject to local minima, this approach reduces intrinsic non-uniqueness of the inverse problem (Colombo and De Stefano, 2007). Some examples of joint inversion studies and data include: cooperative inversion (Lines et al., 1988), weighted schemes for inverting seismic travel times and gravity data (Lees and Vandecar, 1991), DC resistivity and seismic data (Gallardo and Meju, 2004), receiver functions and surface wave dispersion (Bodin et al., 2012; Julia et al., 2000; Sosa et al., 2013; West et al., 2004b), surface wave velocity and gravity observations (Bailey et al., 2012; Liu et al., 2011; Maceira and Ammon, 2009), receiver functions, surface wave dispersion, and magnetotelluric data (Moorkamp et al., 2010; Moorkamp et al., 2011), and topography, Bouguer anomalies, geoid height, and surface heat flow data (Jones et al., 2013). In most of these studies, the main assumption is that the data sets comprised in the inversion complement each other and sample similar geological boundaries.

In this work, we apply a 1-D constrained optimization approach for joint inversion of two complementary data sets, receiver functions and surface waves group dispersion (Julia et al., 2000) using Primal–Dual Interior Point methods as a solver (Sosa et al., 2013). Our approach addresses some of the well known numerical difficulties that arise for large-dimensional model spaces by using inequality constraints to incorporate a priori information and constrain further the geophysical inversion (Sosa et al., 2013).

We characterize the Earth's structure by using S-wave velocities as the model parameter. The forward nonlinear operator $F \in R^m$ evaluated at a given velocity $x \in R^n$ provides a prediction of the Earth's response according to the data used as input. For a given observed data vector, $y \in R^m$, we pose the inverse problem as

$$\min_x \frac{1}{2}\left(\left\| F^{SW}(x) - y^{SW} \right\|_W^2 + \left\| F^{RF}(x) - y^{RF} \right\|_W^2\right), \tag{1}$$

where W represents a weighted diagonal matrix used to equalize the contribution of each data set with respect to physical units and number of data points, while accounting for data set influence (Sosa et al., 2013). In our case, the forward operator, F, collects both the numerical computation of synthetic waveforms for receiver functions, F^{RF} (Ammon, 1991), and the numerical evaluation of surface waves dispersion velocities, F^{SW} (Maceira and Ammon, 2009). We assume a typical uncertainty value σ_i^2 of 0.05 (km/s) for SW, 0.01 (s) for RF observations (Julia et al., 2000), and we accommodate the amount of influence for each data set according to the station data quality. In general, this value is set equal for most of the stations.

Instead of the standard formulation of the inverse problem as in the unconstrained weighted nonlinear least squares (NLSQ) setting (1), we solve a sequence of linearized constrained LSQ with $F'(x_k)$ as the matrix with the partial derivatives of $F(x) = \begin{bmatrix} F^{SW} \\ F^{RF} \end{bmatrix}$. Therefore we rewrite problem (1) as,

$$\min_x \frac{1}{2} \left\| F'(x_k)x + b \right\|_W^2$$
$$\text{s.t.} \quad g(x) \geq 0, \tag{2}$$

where $b = F(x_k) - y - F'(x_k)x_k$ is the residual vector. Here, the inequality constraint defined as

$$g(x) = \begin{cases} x - v_{\min} \\ v_{\max} - x \\ n\gamma - \frac{1}{2}\|Lx\|^2, \end{cases} \qquad \gamma \in (0, v_{\max} - v_{\min}),$$

allows us to add appropriate bounds corresponding to a priori minimum and maximum velocities, i.e. $v_{\min} \leq x \leq v_{\max}$, while enforcing a roughness model constraint by using a first order discrete derivative operator L (Hansen, 2010). The idea of a narrow class of models to be used in the inversion may help the originally ill-posed inverse problem to become well-posed (Zhdanov, 2002). We apply primal–dual interior point (PDIP) methods to solve problem (2), which introduce an intrinsic regularization to the inverse problem making the joint inversion algorithm more robust (Nocedal and Wright, 2006; Sosa et al., 2013). In this method, we define the augmented Lagrangian function associated to (2): $\Gamma(x, z) = \frac{1}{2}\|F'(x_k)x + b\|_W^2 - g(x)^T z$, $z > 0$ where $z \in R^{2n}$ is the Lagrange multiplier corresponding to the inequality constraints.

Interior point methods are based on Newton's method. In our case, the necessary or perturbed Karush–Kuhn–Tucker (KKT) conditions, computed by differentiating Γ with respect to the primal variables x and z, provide the right hand side of a Newton's system. This system can be solved iteratively by using a linesearch strategy (Nocedal and Wright, 2006) while enforcing the iterates to stay in a feasible (interior) region as described in Sosa et al. (2013). The iterative process proceeds until it is either terminated when the misfit is less than 10^{-6}, or a maximum number of iterations – no greater than six – is reached, or the difference between iterates fail to differ more than a threshold of 10^{-5}. For all the stations involved in the geophysical inversion, the initial velocity model, x_0, corresponds to the AK-135 model of Kennett et al. (1995), starting at 10 km depth and distributed at a 2 km interval up to 70 km depth, then at a 5 km interval up to 250 km and finally at 10 km until 300 km.

Since any inversion algorithm produces non-unique results, with ours being no exception, it seems helpful to begin with other information, such as known geological constraints. By incorporating explicit velocity bound constraints with a measure of roughness into the inversion model, and for some of the stations adding a regularization term, our approach can thus produce a better constrained model while having more stable inversions (Sosa et al., 2013).

6. Joint inversion results

We perform 1-D joint inversions using our PDIP approach for 147 stations from USArray and LA RISTRA experiment. In general, each independent joint inversion includes at least 3 receiver function bins created according to an average ray parameter, with a width of approximately 0.01 s/km between 0.04 s/km and 0.07 s/km. The average ray parameter was determined by taking the mean value of the maximum and minimum ray parameter for each station before being used for stacking. The number of receiver functions employed to create these stacks depends on the station, but in general is not less than 25 per ray parameter. Each receiver function consists of 820 data points for a time range from −5 to 80 s. We also include fundamental mode Love and Rayleigh group velocities with 50 to 65 dispersion measurements, with periods between 5 to 140 s. Since the station spacing of the USArray is about 70 km, we anticipate lateral resolution of that order for each individual 1-D inversion in the southern RGR region.

As supplementary material, we present four examples (Figs. S1–S4) in distinct tectonic provinces to show crustal and upper mantle 1-D velocity structure computed by using the constrained joint inversion algorithm: station 118A in the Basin & Range province (Fig. S1), station NM26 in the center of the RGR (Fig. S2), station V18A in the Colorado Plateau (Fig. S3), and station W26A in the Great Plains (Fig. S4). The figures show the fit to the RF observations and the Love and Rayleigh wave group dispersion curves, plus the final model approximation provided by the inversion. Velocity values were extracted from layered models as described before.

7. Kriging interpolation from 1-D velocity profiles

Since our ultimate goal is to create a 3-D Earth structure model of the Rio Grande Rift region, we use the 1-D S wave velocity profiles of each station as input data for a kriging interpolation algorithm (Schultz et al., 1999). In general, interpolation algorithms estimate values by using a weighted sum of surrounding data. Kriging represents an example of a computationally efficient interpolation technique that allows the incorporation of uncertainty on the predicted values. We implement a Bayesian kriging approach that integrates variable spatial damping, a useful tool to control the kriged solution in extrapolation zones where few or no data is available (Schultz et al., 1999). In our case, the station spacing within our region represents a 2-D spatial grid, with each station now having a depth varying 1-D velocity structure. We then can estimate the unknown velocities of the 2-D grid at different depths based on the known velocities, thus creating our 3-D model.

Initially, we remove an appropriate trend prior to applying kriging (Schultz et al., 1999), which, in our case, corresponds to the mean of the velocities at a certain depth. A spatially damped kriging estimator then incorporates variable damping and measurement error multiplied by a unit-normalized function, which decreases noise values to zero according to the prediction's point relative distance. As a result, we obtain a smoothly damping effect over the predicted velocities that varies according to each velocity node and its surroundings. For our results, we choose the blending functions of 2° to guarantee good spatial sampling.

Interpolating the 1-D profiles by means of kriging can help us to illuminate better the Earth structure beneath each station in the RGR. Schematically, if each station had perfect azimuthal coverage, the region below each station would have cone shaped raypaths, where at a certain depth (that depends on station spacing), the raypaths at adjacent stations begin to overlap, providing us with full subsurface structure coverage. Before this depth, we expect that the surface wave group dispersion information obtained from regional earthquakes can improve the av-

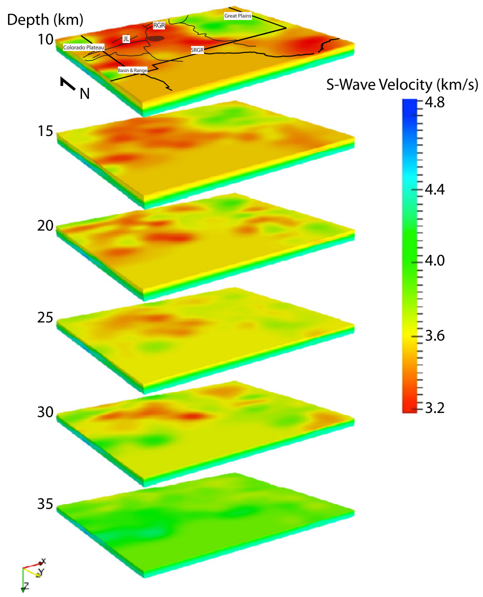

Fig. 5. Crustal slices at different depths from 10 km up to 35 km illustrating various *S* wave velocity models. We use a color scale (maximum to minimum velocities) to highlight crustal anomalies within the Basin & Range, Jemez Lineament (JL), Great Plains, and Southern Rio Grande Rift (SRGR) indicated by the labels on top of the first shear wave model at 10 km depth. We can clearly see a distinct pattern (black arrow) that is consistent throughout the different tectonic provinces in the crustal slices from 10 km to 30 km depth.

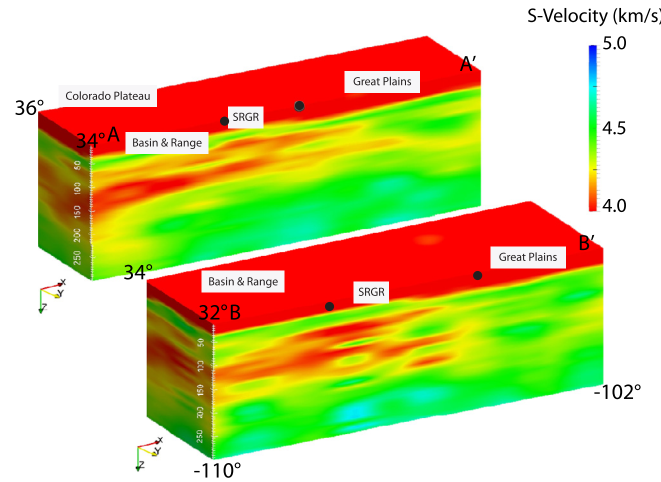

Fig. 6. (Top) Cross-section A–A′ at latitude 34° shows a clear distinction between the Colorado Plateau (CP), Socorro Magma Body at the center of the RGR (middle spheres), and the Great Plains (GP). We find that near the CP there is a mantle lid between 100–150 km (red anomaly) as in Gao et al. (2004) and West et al. (2004a), and the presence of cold mantle lithosphere about 200 km below the Great Plains. Anomalously high velocities begin to appear right below the RGR and continue east of the GP between the depths of 200–300 km. (Bottom) Cross-section B–B′ at latitude 32° covering the southernmost part of the RGR region. We image a low velocity zone that begins to appear beneath the RGR extending to the west below the Basin & Range and Colorado Plateau. Both cross sections show slightly uplifted Moho beneath the Basin & Range province, and a lower and middle crust that might be related to magmatic activity in the upper mantle. (For interpretation of the references to color in this figure, the reader is referred to the web version of this article.)

erage crustal velocity structure and also the vertical resolution (Schmedes et al., 2012). In this fashion, we account for velocity structure resolution avoiding additional inversions by grouping the 1-D profiles depending on azimuthal range as indicated by Bailey et al. (2012). Generally, the upper mantle of a tectonically active region is expected to exhibit 3-D heterogeneities with a length scale smaller than both the lateral resolution of surface waves and vertical resolution of receiver functions (Obrebski et al., 2010). Therefore, the models obtained by using these two data sets should resolve the main features beneath the region of study.

8. 3-D RGR S-wave velocity model

Figs. 5 through 8 show different perspectives of the resulting 3-D crustal and upper mantle structure images, including the profiles presented in Fig. 2. For Fig. 5, we use a color scale (maximum to minimum velocities) to highlight crustal anomalies and a different color scale in Figs. 6 through 8 with a reduced color spectrum varying from 4.0 km/s to 5 km/s, similar to that used by West et al. (2004a), to highlight mantle anomalies.

Fig. 5 shows depth slices from 10 to 35 km that highlight crustal anomalies in our model. The rift can be seen in the crust with low velocities along its axis from north to south, from 10 to 30 km in depth. The rift appears with a uniformly slow mantle under the RGR and its surroundings, and seems to continue southeast along the Texas–Mexico border, yet we have no resolution south of the border.

Fig. 6 shows our 3-D velocity model at cross-section A–A′ and B–B′. The ∼740 km long cross section A–A′ coincides with latitude 34°, and passes through Colorado Plateau, Socorro Magma Body (SMB) and ends at the Great Plains. Cross-section B–B′ coincides with latitude 32° and covers the southernmost part of the study area. Both cross sections show slightly uplifted Moho beneath the Basin & Range province, and a lower and middle crust that might be related to magmatic activity in the upper mantle. Gao et al. (2004) relate this activity to convection in the deeper mantle. This area of active upper crust extension is suggested to be primarily the product of magmatic activity in the lower crust and upper mantle (Serpa et al., 1988). Beneath the Colorado Plateau, Fig. 6 also shows a mantle lid between 100–150 km as in Gao et al. (2004) and West et al. (2004a), and the presence of cold mantle lithosphere about 200 km below the Great Plains. Van Wijk et al. (2008) explained these strong fast anomalies at the western edge of the Great Plains thermally as cold downwelling lithosphere destabilized by small-scale convection.

To further investigate the upper mantle of our model, Fig. 7 shows depth slices from 50 to 300 km depth in 50 km intervals. At 50 km and 100 km depth, a low velocity anomaly is present north of 34° and appears affiliated with the Jemez lineament. However, another low velocity anomaly in the southern RGR appears from 50 to 150 km. This anomaly may be connected with the Jemez lineament, but its persistence and narrowness signifies a possible upwelling. These anomalies appear to terminate at 200 km depth, with no strong signatures from 200–300 km.

Cross-section C–C′ (Fig. 8) is ∼700 km long to coincide with the southern part of the Rio Grande Rift (LA RISTRA) experiment and cross cut the profiles A–A′, and B–B′. The transect begins at Colorado Plateau, passes through the SMB and ends west of the southern RGR. We identify an upper mantle low velocity feature beneath the Jemez lineament, which may originate outside our study area and is present in Fig. 7 north of 34° latitude. Gao et al. (2004) discussed the possible presence of an eastward flow of mantle from the Jemez region across the rift with sinking beneath the Great Plains. Furthermore, West et al. (2004a) state that to the west of the Great Plains, an asthenospheric low velocity channel underlies the region and extends to 150 km depth. This low velocity zone continues further to the Colorado Plateau at 100–200 km depth. This is similar to what West et al. (2004a) describe, except that we do identify it directly beneath the Rift and it does not form an inverted U-shape. Instead, we see an oblique body that may continue outside our study region, which we term the Jemez Upwelling, that is present in profiles A–A′ and B–B′. The difference

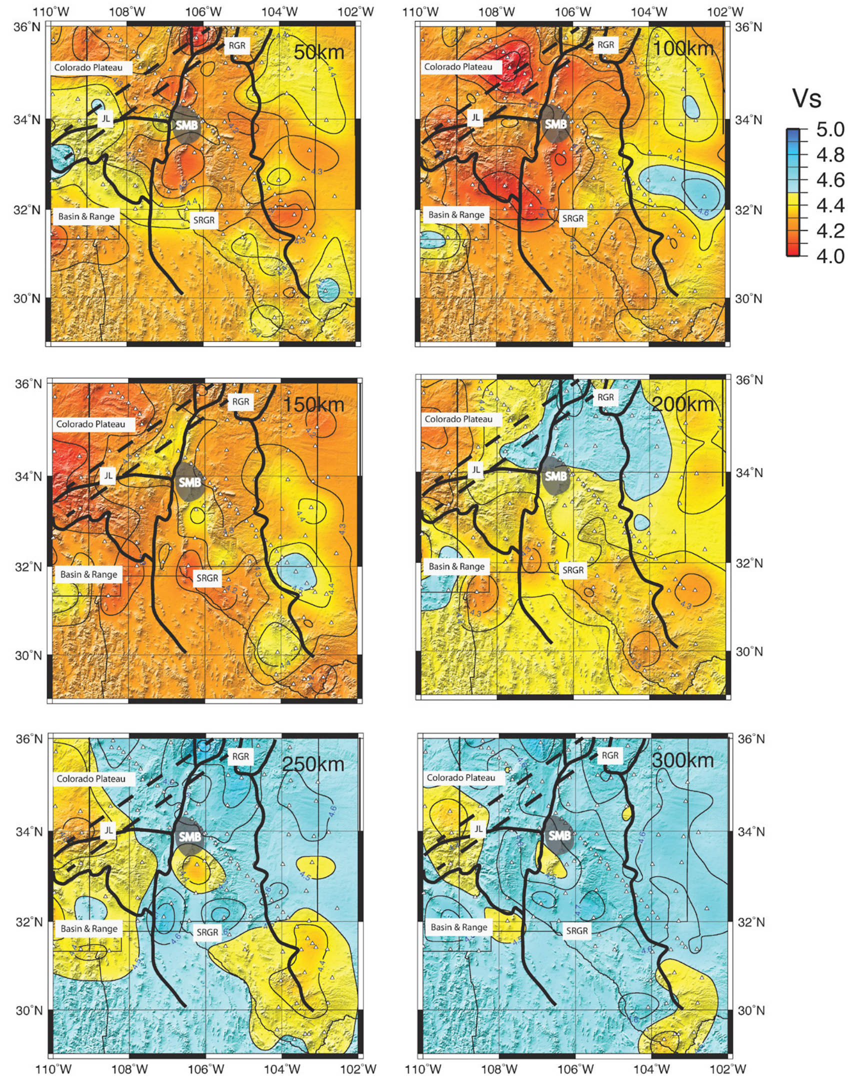

Fig. 7. Shear wave velocity maps at different depths starting at 50 km up to 300 km. We identify an upper mantle low velocity feature beneath the Jemez lineament, which may originate outside our study area. At 50 km and 100 km depth, a low velocity anomaly is present north of 34° and seems to be affiliated with the Jemez lineament. However, another low velocity anomaly in the southern RGR appears from 50 to 150 km. This anomaly may be connected with the Jemez lineament, but its persistence and narrowness signifies a possible upwelling. These anomalies appear to terminate at 200 km depth, with no strong signatures from 200–300 km.

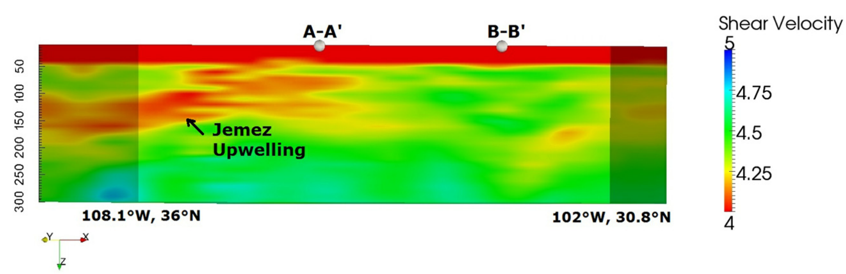

Fig. 8. Cross-section C–C′ coincides with the southern part of the LA RISTRA passive experiment. Seismically fast mantle underlies the RGR and relatively slow mantle is seen beneath the Mt. Taylor and Colorado Plateau. We identify an upwelling beneath the Jemez Lineament, which we term the Jemez Upwelling. The anomalously high velocities beneath the RGR appear to decrease at both sides of the rift, particularly beneath the GP portion.

between our results and West et al. (2004a) is likely the result of different approaches and assumptions, but the 3-D nature of our results further clarify the anomaly, which we discuss below.

Reviewing the 3-D models in Figs. 6 and 8, we find no evidence for a deep mantle source under the Rift, implying that it is not currently driven by deep mantle upwelling (Wilson et al., 2005a; West et al., 2004a). However, Moucha et al. (2008) suggest that this interpretation was based on static images that could not assess the level of flow beneath the RGR. Based on their flow simulations, Moucha et al. (2008) propose that the mantle flow below the RGR is associated with thermal upwelling. As in previous studies, we image not only the low velocity mantle beneath the RGR (Gao et al., 2004; Roy et al., 2005; West et al., 2004a; Wilson et al., 2010), but also sharp changes between the RGR and the two surrounding provinces of Basin & Range and Colorado Plateau (Bailey et al., 2012). Along the RGR, although resolution is reduced at depth, we see no persistent low velocity anomaly deeper than 200 km.

9. Discussion

Comparing our 3-D model directly to others can be difficult and requires complete visualization of all models in one figure (e.g., Becker, 2012; Pavlis et al., 2012). Since our models were derived from 1-D inversions of two complementary data sets that were then interpolated to 3-D, we expected to find differences in our 3-D model compared to previous studies. We also focus solely in this region, while many of the other models include much larger regions (Gilbert, 2012; Levander and Miller, 2012; Moucha et al., 2008; Sine et al., 2008; van Wijk et al., 2008). Thus, we show features relevant to RGR evolution, and highlight those that we believe are fully consistent with the most recent and past models in the southern Rio Grande Rift obtained by using different data sets and techniques. We discuss below the impact of the PDIP approach, the new model for the southern RGR, and finally highlight the main new feature not highlighted in other work: the Jemez Upwelling and the SRGR low velocity anomaly.

9.1. PDIP methodology

We implement a new approach for joint inversion of receiver function and surface wave group dispersion data based on constrained optimization (Sosa et al., 2013). We create independent 1-D Earth velocity profiles of upper mantle velocity structure along the southern RGR. In general, no smoothing or damping factors were used to stabilize the inversions. This is an advantage when compared to other standard techniques, which often require tuning of several regularization parameters. It is well known that for severely ill-posed inversions that may appear for some stations, determining the optimum regularization parameters remain as a difficult and often speculative task (Sosa et al., 2013; Zhdanov, 2002). There are several strategies to choose these regularization parameters (Hansen, 2010; Zhdanov, 2002), and some recent advances on transdimensional inversion to include them directly as inversion parameters (Bodin et al., 2012). However, there is not yet an analytical or automatic way to find the best parameter for all particular cases (Hansen, 2010; Moorkamp et al., 2011). The PDIP approach reduces the subjectivity of these selections, since when necessary the simple inclusion of a damping parameter stabilizes the inversion (Sosa et al., 2013).

Some stations have inversion convergence issues mostly due to the absence of good quality RF data to identify absolute *S*-wave velocities and sharp discontinuities. Those stations were independently tuned by using several damping factors. We note that to obtain improvements, a damping factor of 0.1 and an influence parameter equal to 0.25 was necessary. Furthermore, we found that in some cases even modifying the influence parameter to be 0.75, the damping factor did not improve the numerical results for the problematic stations. We discuss with detail the impact of regularization (damping/smoothing) on our constrained optimization approach in Sosa et al. (2013).

Bailey et al. (2012) use a similar approach combining results obtained by independent joint inversion of surface wave phase velocities and receiver function information, to compute 1-D *S* wave velocity profiles for the Colorado Plateau. They extracted common features of nearby stations that were reconciled with observed gravity anomalies. The anomalies are then established by using empirical relations to density structure. Bailey et al. (2012) state that by creating 3-D images of Earth structure based on independent inversions that produce 1-D velocity profiles, the results are likely inferior compared to a full 3-D parameter approach. However, a 3-D inversion involves a high volume of information and a great number of parameters, which may be numerically intractable. PDIP methods on the other hand have been proven to be successful in solving large-scale problems (Nocedal and Wright, 2006), and we will explore the migration of our technique to a full 3-D inversion in future work.

We can adjust our inversion approach by tuning the kriging interpolation blending function according to the geological province where the stations are located, e.g. Basin and Range, RGR, Great Plains, as an attempt to enhance the performance of the inversion algorithm. However, our approach allows us to begin with a standard initial model (ak135: Kennett et al., 1995), and produce coherent independent inversions that could be combined for a consistent 3-D structure. This represents another difference to the approach presented by Bailey et al. (2012), where they weight the contribution of each inversion separately to select a suitable initial model.

9.2. Interpretation: Basin and Range, Colorado Plateau, RGR, and Great Plains

Roy et al. (2005) argue that the RGR and southeastern Colorado Plateau is underlain by a low-density upper mantle province, which does not trend along upper crustal tectonic boundaries, but correlates with regions of late Tertiary magmatism. The Rio Grande Rift system is characterized by anomalously high topography (Roy et al., 2005) and its crustal thickness is thick along its eastern flank and thin in its center (Keller, 2004). As in Bailey et al. (2012), we observe sharp changes in crustal thickness that distinguish between the Colorado Plateau and surrounding provinces dominated by extension, e.g. BR, GP and RGR. Roy et al. (2005) showed that low wave speed zones are broad in the north and narrow in the south. We find a low velocity zone at depths from 100–150 km that coincides with the southernmost RGR. Reiter and Chamberlin (2011) concluded that the LA RISTRA profile experiment showed evidence of mantle convection and partial melting in the crust and upper mantle. Although we have no conclusive evidence of melting, we see higher velocities in some regions (Fig. 6) at latitude 34° and along the LA RISTRA profile (Fig. 8).

We image similar *S* wave velocities as the LA RISTRA profile (50–250 km), yet we do not have a “bow-tie” low velocity anomaly (Gao et al., 2004; West et al., 2004b; Wilson et al., 2005a). The layering seen in Fig. 6 to the north of AA′ and BB′ may be evidence of delamination. Initially, delamination was proposed as one of the main alternative mechanisms of lithospheric recycling in continental collision areas (Bird, 1979). In a pure rift system, we would expect thinned crust and absent or thinned lithosphere. Without a large convection upwelling, observation of a thin crust and lithosphere together with high heat flow may suggest that the lower crust has been removed through delamination (Levander et al., 2011). The delamination process can ultimately lead to considerable thickening of the crust by underplating in areas with weak lithosphere (Fig. 7). Bashir et al. (2011), however, suggested that crustal thinning of the BR was a result of simple stretching of the original crust rather than delamination. We do find thin crust under this province, but we cannot conclude whether the origin of such feature is either delamination or simply stretching of the crust.

9.3. The Jemez upwelling and the southern RGR anomaly

The Jemez lineament, an alignment of volcanic centers that extends about 800 km (Fig. 2) (Aldrich, 1986; Goff and Janik, 2002), represents the most important signature of primary volcanism in the region of the Rio Grande Rift (Spence and Gross, 1990). The Jemez lineament formed from the Miocene to Holocene in what is thought to be a reactivated Precambrian structure (Aldrich, 1986;

Goff and Janik, 2002). Using the results of a reconnaissance experiment of lateral variation for P-wave velocities, Spence and Gross (1990) identified a low velocity zone along the Jemez lineament in the depth range from 50–200 km and interpreted the zone to be partial melt. However, the resolution of their model lies beneath the ~200-km-long segment from Mount Taylor through the Jemez volcanic center, and up to 160 km depth only. This feature shows up in other tomography models in the region, where a low velocity anomaly is present until about 200–300 km in depth (Gao et al., 2004; Moucha et al., 2008; van Wijk et al., 2008)

We identify the same low velocity zone to a 200 km depth. With a 3-D perspective, we link the low velocity zone to an upwelling sheet of hot (low velocity) material, which we term the Jemez upwelling, beneath the Jemez lineament originating beneath the Colorado Plateau, and that likely feeds the volcanic centers in the region (Fig. 7). This feature may be linked to the southern RGR low velocity anomaly (Fig. 6) at 100 km depth along the axis of the rift. However, the southern RGR anomaly appears to be narrower than the Jemez upwelling and may extend up to 150 km. Moucha et al. (2008) suggest that strong upwelling impacts the base of the lithosphere at an oblique angle east of the Colorado Plateau and directly below the RGR. The planar body parallels the Jemez lineament and is oriented perpendicular to the LA RISTRA transect (C–C′).

Along the C–C′ transect, our results are similar to previous images for the LA RISTRA experiment, where a significant transition between high velocities beneath the Colorado Plateau and the Great Plains is revealed as well as a broad low velocity zone beneath the RGR (Gao et al., 2004; Wilson et al., 2005a). Furthermore, our 3-D images allow us to define the dimensions of the low velocity zone in our region and to link this Jemez upwelling to the Jemez lineament. However, due to the northern extent of our model, we do not know if the low velocity zone is persistent beneath the Colorado Plateau (Gao et al., 2004; West et al., 2004a).

The Socorro Magma Body (SMB) within central RGR is one of the largest active intrusions in the Earth's continental crust, and is associated to steady central uplift (Pearse and Fialko, 2010). Also, the SMB has been linked to strong magma influence, e.g. diffusion of fluid moving upward from depth, due to an underlying low-velocity molten layer. Roy et al. (2005) associated this low velocity zone to a possible combination of partial melt, temperature and compositional variations. Ruhl et al. (2010) suggested that there is not a strong direct magmatic influence in the seismic activity of the SMB, and that this activity is more prone to be associated with characteristics of a continental rift, like preexisting highly fractured crust. Furthermore, the strongest velocity variations located in the upper 200–300 km of mantle beneath the magmatically and tectonically active Rio Grande Rift and Basin and Range show a clear relation between tectonic province and mantle velocity beneath the stable Great Plains (Fig. 6). This distinction coincides with that presented by Gao et al. (2004) and Wilson et al. (2005a). The RGR can clearly been seen as a strong crustal feature in our models (Fig. 5), while the two major low velocity zones in our model (the Jemez Lineament and the southern RGR anomaly) highlight an upper mantle process that may be there result of small-scale convection (Figs. 5–8). However, because a deep mantle upwelling underneath the RGR does not appear, the mechanism for rift formation remains ambiguous.

10. Conclusions

We present a new model of crustal and upper mantle structure beneath the southern RGR. Separate joint inversions were performed for 147 Earthscope USArray and LA RISTRA stations. We create a framework that connects a constrained optimization joint inversion algorithm with a Bayesian interpolation scheme for high resolution imaging of earth structure. Furthermore, this scheme efficiently provides a robust alternative to extend simultaneous independently created 1-D S wave velocity models, to produce 3-D images of Earth's structure as opposed to full 3-D inversions. Our framework generates a continuous and smooth 3-D velocity model of the Rift system, revealing the complexities of the southern RGR and helping us to better characterize its crustal and upper mantle velocity structure. We present evidence of crustal thinning in the center of the Rift, and no evidence of a deep mantle upwelling driving the RGR (Gao et al., 2004). We identify the boundaries between the provinces of B&R, CP, GP and RGR, and an upwelling sheet of low velocity material, that we term the Jemez upwelling. We also identify a southern RGR anomaly that may be connected with the Jemez upwelling. The resulting 3-D models show a thin, lower velocity crust along the southern east portion of the Rio Grande Rift, plus a low velocity lithosphere underneath the Colorado Plateau and Basin and Range province which may be attributed to high crustal temperatures (Bensen et al., 2009). We have no evidence of a deep mantle plume that drives the current rifting process, and all velocity anomalies are shallower than 200 km.

Acknowledgements

This research project is based on work supported by the National Science Foundation under Grant No. 0734825, and the Program in Computational Science. We thank the Department of Geological Sciences. This manuscript was significantly improved with comments from Peter Shearer and two anonymous reviewers.

Appendix A. Supplementary material

Supplementary material related to this article can be found online at http://dx.doi.org/10.1016/j.epsl.2014.06.002.

References

Abt, D.L., Fischer, K.M., French, S.W., Ford, H.A., Yuan, H., Romanowicz, B., 2010. North American lithospheric discontinuity structure imaged by Ps and Sp receiver functions. J. Geophys. Res. 115, B09301. http://dx.doi.org/10.1029/2009JB006914.

Aldrich, M.J., 1986. Tectonics of the Jemez lineament in the Jemez Mountains and the Rio Grande Rift. J. Geophys. Res. 91, 1753–1762.

Ammon, C.J., 1991. The isolation of receiver effects from teleseismic P wave forms. Bull. Seismol. Soc. Am. 81, 2504–2510.

Averill, M.G., Miller, K.C., Keller, G.R., Kreinovich, V., Araiza, R., Starks, S.A., 2007. Using expert knowledge in solving the seismic inverse problem. Int. J. Approx. Reason. 45, 564–587.

Bailey, I.W., Miller, M.S., Liu, K.J., Levander, A., 2012. V-S and density structure beneath the Colorado Plateau constrained by gravity anomalies and joint inversions of receiver function and phase velocity data. J. Geophys. Res., Solid Earth 117, B04404. http://dx.doi.org/10.1029/2011JB008943.

Bashir, L., Gao, S.S., Liu, K.H., Mickus, K., 2011. Crustal structure and evolution beneath the Colorado Plateau and the southern Basin and Range Province: Results from receiver function and gravity studies. Geochem. Geophys. Geosyst. 12, Q06008. http://dx.doi.org/10.1029/2011GC003563.

Becker, T.W., 2012. On recent seismic tomography for the western United States. Geochem. Geophys. Geosyst. 13, Q01W10. http://dx.doi.org/10.1029/2011GC003977.

Bensen, G.D., Ritzwoller, M.H., Yang, Y., 2009. A 3-D shear velocity model of the crust and uppermost mantle beneath the United States from ambient seismic noise. Geophys. J. Int. 177 (3), 1177–1196.

Berglund, H.T., Sheehan, A.F., Murray, M.H., Roy, M., Lowry, A.R., Nerem, R.S., Blume, F., 2012. Distributed deformation: the Rio Grande Rift, Great Plains and Colorado Plateau. Geology 40 (1), 23–26.

Bird, P., 1979. Continental delamination and the Colorado Plateau. J. Geophys. Res. 84, 7561–7571.

Bodin, T., Sambridge, M., Tkalčić, H., Arroucau, P., Gallagher, K., Rawlinson, N., 2012. Transdimensional inversion of receiver functions and surface wave dispersion. J. Geophys. Res. 117 (B2). http://dx.doi.org/10.1029/2011JB008560.

Buehler, J.S., Shearer, P.M., 2010. Pn tomography of the western United States using USArray. J. Geophys. Res. 115, B09315. http://dx.doi.org/10.1029/2009JB006874.

Buehler, J.S., Shearer, P.M., 2012. Localized imaging of the uppermost mantle with USArray Pn data. J. Geophys. Res. 117, B09305. http://dx.doi.org/10.1029/2012JB009433.

Burdick, S., Van der Hilst, R.D., Vernon, F.L., Martynov, V., Cox, T., Eakins, J., Karasu, G.H., Tyllel, J., Astiz, L., Pavlis, G.L., 2010. Model update January 2010: upper mantle heterogeneity beneath North America from traveltime tomography with global and USArray Transportable Array data. Seismol. Res. Lett. 81, 689–693.

Cao, A., Levander, A., 2010. High-resolution transition zone structures of the Gorda Slab beneath the western United States: Implication for deep water subduction. J. Geophys. Res., Solid Earth (1978–2012) 115 (B7).

Chapin, C.E., Cather, S.M., 1994. Tectonic setting of the axial basins in the northern and central Rio Grande Rift. In: Keller, Randy G., Cather, Steven M. (Eds.), Basins of the Rio Grande Rift: Structure, Stratigraphy, and Tectonic Setting. In: GSA Special Paper, vol. 291, pp. 5–25.

Cho, K.H., Herrmann, R.B., Ammon, C.J., Lee, K., 2007. Imaging the upper crust of the Korean Peninsula by surface-wave tomography. Bull. Seismol. Soc. Am. 97 (1B), 198–207.

Collins, E.W., Raney, J.A., 1994. Tertiary and Quaternary tectonics of the Hueco Bolson, Trans-Pecos Texas and Chihuahua, Mexico. In: Keller, G.R., Cather, S.M. (Eds.), Basins of the Rio Grande Rift; Structure, Stratigraphy, Setting, Tectonic. In: GSA Special Papers, vol. 291, pp. 265–282.

Colombo, D., De Stefano, M., 2007. Geophysical modeling via simultaneous joint inversion of seismic, gravity, and electromagnetic data: application to prestack depth imaging. Lead. Edge 26, 326–331.

Cook, F.A., Decker, E.R., Smithson, S.B., 1978. Preliminary transient heat flow model of the Rio Grande Rift, Southern New Mexico. Earth Planet. Sci. Lett. 40, 316–326.

Dugda, M.T., Nyblade, A.A., Julia, J., Langston, C.A., Ammon, D.J., Simiyu, S., 2005. Crustal structure in Ethiopia and Kenya from receiver function analysis: Implications for rift development in eastern Africa. J. Geophys. Res. 110, 1–15.

Gallardo, L.A., Meju, M.A., 2004. Joint two-dimensional DC resistivity and seismic traveltime inversion with cross-gradients constraints. J. Geophys. Res. 109, B03311. http://dx.doi.org/10.1029/2003JB002716.

Gao, W., Grand, S.P., Baldridge, W.S., Wilson, W.S., West, M., Ni, J.F., Aster, R., 2004. Upper mantle convection beneath the central Rio Grande Rift imaged by P and S wave tomography. J. Geophys. Res. 109, B03305. http://dx.doi.org/10.1029/2003JB002743.

Gilbert, H., 2012. Crustal structure and signatures of recent tectonism influenced by ancient terranes in the western United States. Geosphere 8, 141–157. http://dx.doi.org/10.1130/GES00720.1.

Gilbert, H., Velasco, A.A., Zandt, G., 2007. Preservation of Proterozoic terrane boundaries within the Colorado Plateau and implications for its tectonic evolution. Earth Planet. Sci. Lett. 258, 237–248.

Goff, F., Janik, C.J., 2002. Gas geochemistry of the Valles Caldera region, New Mexico and comparisons with gases at Yellowstone, Long Valley and other geothermal systems. J. Volcanol. Geotherm. Res. 116, 299–323.

Hansen, P.C., 2010. Discrete Inverse Problems. SIAM.

Hansen, S.M., Dueker, K.G., Stachnik, J.C., Aster, R.C., Karlstrom, K.E., 2013. A rootless rockies – support and lithospheric structure of the Colorado Rocky Mountains inferred from CREST and TA seismic data. Geochem. Geophys. Geosyst. 14, 2670–2695. http://dx.doi.org/10.1002/ggge.20143.

Herrmann, R.B., Ammon, C.J., 2002. Computer programs in seismology. Version 3.30. Saint Louis University.

Herrmann, R.B., Ammon, C.J., Benz, H., 2013. Group Velocity Dispersion for North America. http://www.eas.slu.edu/eqc/eqc_research/NATOMO.

Jones, A.G., Alfonso, J.C., Fullea, J., Salajegheh, F., 2013. The lithosphere–asthenosphere system beneath Ireland from integrated geophysical–petrological modeling — I: Observations, 1D and 2D hypothesis testing and modeling. Lithos. http://dx.doi.org/10.1016/j.lithos.2013.10.033.

Julia, J., Ammon, C.J., Herrmann, R., Correig, M., 2000. Joint inversion of receiver function and surface wave dispersion observations. Geophys. J. Int. 142, 99–112.

Keller, G.R., 2004. Geophysical constraints on the crustal structure of New Mexico. In: Mack, G.H., Giles, K.A. (Eds.), The Geology of New Mexico, A Geologic History. In: New Mexico Geological Society, Special Publication, vol. 11, pp. 439–456 (invited contribution).

Keller, G.R., Baldridge, W.S., 1999. The Rio Grande Rift: a geological and geophysical overview. Rocky Mt. Geol. 34, 121–130.

Keller, G.R., Morgan, P., Seager, W.R., 1990. Crustal structure, gravity anomalies, and heat flow in the southern Rio Grande Rift and their relationship to extensional tectonics. Tectonophysics 174, 21–37.

Keller, G.R., Khan, M.A., Morgan, P., Wendlandt, R.F., Baldridge, W.S., Olsen, K.H., Prodehl, C., Braile, L.W., 1991. A comparative study of the Rio Grande and Kenya Rifts. In: Gangi, A.F. (Ed.), World Rift Systems. In: Tectonophysics, vol. 197, pp. 355–371.

Kennett, B.L.N., Engdahl, E.R., Buland, R., 1995. Constraints on seismic velocities in the Earth from traveltimes. Geophys. J. Int. 122 (1), 108–124.

Kreemer, C., Blewitt, G., Bennett, R.A., 2010. Present-day motion and deformation of the Colorado Plateau. Geophys. Res. Lett. 37, L10311. http://dx.doi.org/10.1029/2010GL043374.

Kumar, P., Kind, R., Yuan, X., Mechie, J., 2012. USArray receiver function images of the lithosphere–asthenosphere boundary. Seismol. Res. Lett. 83 (3), 486–491. http://dx.doi.org/10.1785/gssrl.83.3.486.

Langston, C.A., 1981. Evidence for the subducting lithosphere under southern Vancouver Island and western Oregon from teleseismic P wave conversions. J. Geophys. Res. 86, 3857–3866.

Lees, J.M., Vandecar, J.C., 1991. Seismic tomography constrained by Bouguer gravity anomalies: applications in western Washington. Pure Appl. Geophys. 135, 31–52.

Levander, A., Miller, M.S., 2012. Evolutionary aspects of lithosphere discontinuity structure in the western US. Geochem. Geophys. Geosyst. 13, Q0AK07. http://dx.doi.org/10.1029/2012GC004056.

Levander, A., Schmandt, B., Miller, M.S., Liu, K., Karlstrom, K.E., Crow, R.S., Lee, C.-T.A., Humphreys, E.D., 2011. Continuing Colorado plateau uplift by delamination-style convective lithospheric downwelling. Nature 472, 461–466.

Lin, F.-C., Schmandt, B., Tsai, V.C., 2012. Joint inversion of Rayleigh wave phase velocity and ellipticity using USArray: constraining velocity and density structure in the upper crust. Geophys. Res. Lett. 39, L12303. http://dx.doi.org/10.1029/2012GL052196.

Lines, L.R., Schultz, A.K., Treitel, S., 1988. Cooperative inversion of geophysical data. Geophysics 53, 8–20.

Liu, L., Gurnis, M., 2010. Dynamic subsidence and uplift of the Colorado Plateau. Geology 38, 663–666.

Liu, K., Levander, A., Niu, F., Miller, M.S., 2011. Imaging crustal and upper mantle structure beneath the Colorado Plateau using finite frequency Rayleigh wave tomography. Geochem. Geophys. Geosyst. 12, Q07001. http://dx.doi.org/10.1029/2011GC003611.

Lodge, A., Helffrich, G., 2009. Grid search inversion of teleseismic receiver functions. Geophys. J. Int. 178, 513–523.

Maceira, M., Ammon, C.J., 2009. Joint inversion of surface wave velocity and gravity observations and its application to central Asian basins s-velocity structure. J. Geophys. Res. 114, B02314. http://dx.doi.org/10.1029/2007JB0005157.

Machette, M.N., 1998. Contrasts between short- and long-term records of seismicity in the Rio Grande rift; important implications for seismic-hazard assessments in areas of slow extension. In: Lund, W.R. (Ed.), Proceedings Volume; Basin and Range Province Seismic-Hazards Summit. In: Misc. Pub. - Utah Geo. Survey, vol. 98-2, pp. 84–95.

Miller, M.S., Eaton, D.W., 2010. Formation of cratonic mantle keels by arc accretion: evidence from S receiver functions. Geophys. Res. Lett. 37, L18305. http://dx.doi.org/10.1029/2010GL044366.

Moorkamp, M., Jones, A.G., Fishwick, S., 2010. Joint inversion of receiver functions, surface wave dispersion, and magnetotelluric data. J. Geophys. Res. 115, B04318. http://dx.doi.org/10.1029/2009JB0006369.

Moorkamp, M., Heincke, B., Jegen, M., Roberts, A.W., Hobbs, R.W., 2011. A framework for 3-D joint inversion of MT, gravity and seismic refraction data. Geophys. J. Int. 184, 477–493.

Moschetti, M.P., Ritzwoller, M.H., Lin, F.-C., Yang, Y., 2010. Crustal shear wave velocity structure of the western United States inferred from ambient seismic noise and earthquake data. J. Geophys. Res. 115, B10306. http://dx.doi.org/10.1029/2010JB007448.

Moucha, R., Forte, A.M., Rowley, D.B., Mitrovica, J.X., Simmons, N.A., Grand, S.P., 2008. Mantle convection and the recent evolution of the Colorado Plateau and the Rio Grande Rift valley. Geology 36 (6), 439–442.

Moucha, R., Forte, A.M., Rowley, D.B., Mitrovica, J.X., Simmons, N.A., Grand, S.P., 2009. Deep mantle forces and the uplift of the Colorado Plateau. Geophys. Res. Lett. 36, L19310. http://dx.doi.org/10.1029/2009GL039778.

Nocedal, J., Wright, S.J., 2006. Numerical Optimization, 2nd edition. Springer-Verlag.

Obrebski, M., Kiselev, S., Vinnik, L., Montagner, J.-P., 2010. Anisotropic stratification beneath Africa from joint inversion of SKS and P receiver functions. J. Geophys. Res. 115, B09313. http://dx.doi.org/10.1029/2009JB006923.

O'Driscoll, L.J., Humphreys, E.D., Schmandt, B., 2011. Time corrections to teleseismic P delays derived from SKS splitting parameters and implications for western U.S. P-wave tomography. Geophys. Res. Lett. 38, L19304. http://dx.doi.org/10.1029/2011GL049031.

Pavlis, G.L., Sigloch, K., Burdick, S., Fouch, M.J., Vernon, F.L., 2012. Unraveling the geometry of the Farallon plate: synthesis of three-dimensional imaging results from USArray. Tectonophysics 532–535, 82–102.

Pearse, J., Fialko, Y., 2010. Mechanics of active magmatic intraplating in the Rio Grande Rift near Socorro, New Mexico. J. Geophys. Res. 115, B07413. http://dx.doi.org/10.1029/2009JB006592.

Reiter, M., Chamberlin, R.M., 2011. Alternative perspective of crustal and upper mantle phenomena along the Rio Grande Rift. GSA Today 21, 4–9.

Roy, M., MacCarthy, J.K., Selverstone, J., 2005. Upper mantle structure beneath the eastern Colorado Plateau and Rio Grande Rift revealed by Bouguer gravity, seismic velocities, and xenolith data. Geochem. Geophys. Geosyst. 6, 10.

Roy, M., Jordan, T.H., Pederson, J., 2009. Colorado Plateau magmatism and uplift by warming of heterogeneous lithosphere. Nature 459, 978–982.

Ruhl, C., Bilek, S.L., Stankova-Pursley, J., 2010. Relocation and characterization of the August 2009 microearthquake swarm above the Socorro magma body in the central Rio Grande Rift. Geophys. Res. Lett. 37, L23304. http://dx.doi.org/10.1029/2010GL045162.

Schmedes, J., Roth, J.B., Saltzer, R.L., Leahy, G.M., 2012. Imaging the shallow crust using teleseismic tomography. Bull. Seismol. Soc. Am. 102 (3), 1276–1322.

Schultz, C.A., Myers, S.C., Hipp, J., Young, C.J., 1999. Nonstationary bayesian kriging: a predictive technique to generate spatial corrections for seismic detection, location, and identification. Bull. Seismol. Soc. Am. 88, 1275–1288.

Serpa, L.D., deVoogd, B., Wright, L.A., Willemin, J., Oliver, J.E., Hauser, E.C., Troxel, B.W., 1988. Structure of the Central Death Valley Pull-Apart Basin and Vicinity from COCORP Profiles in the Southern Great Basin. Geol. Soc. Am. Bull. 100, 1437–1450.

Shearer, P.M., 2009. Introduction to Seismology. Cambridge University Press.

Sigloch, K., 2011. Mantle provinces under North America from multifrequency P wave tomography. Geochem. Geophys. Geosyst. 12, Q02W08. http://dx.doi.org/10.1029/2010GC003421.

Sine, C.R., Wilson, D., Gao, W., Grand, S.P., Aster, R., Ni, J., Baldridge, W.S., 2008. Mantle structure beneath the western edge of the Colorado Plateau. Geophys. Res. Lett. 35 (10), L10303.

Song, T., Helmberger, D.V., 2007. A depleted, destabilized continental lithosphere Near the Rio Grande Rift. Earth Planet. Sci. Lett. 262, 175–184.

Sosa, A., Velasco, A.A., Velazquez, L., Argaez, M., Romero, R., 2013. Constrained optimization schemes for geophysical inversion of seismic data. Geophys. J. Int. http://dx.doi.org/10.1093/gji/ggt326.

Spence, W., Gross, R.S., 1990. A tomographic glimpse of the upper mantle source of magmas of the Jemez lineament, New Mexico. J. Geophys. Res. 95 (B7), 10,829–10,849. http://dx.doi.org/10.1029/JB095iB07p10829.

Steck, L.K., Begnaud, M.L., Phillips, S., Stead, R., 2011. Tomography of crustal P and S travel times across the western United States. J. Geophys. Res. 116, B11304. http://dx.doi.org/10.1029/2011JB008260.

Stein, S., Wysession, M., 2009. An Introduction to Seismology, Earthquakes, and Earth Structure. Wiley.

Thompson, L., Velasco, A.A., Hussein, M., submitted for publication. Geophysical constraints on the crustal structure of the Southern Rio Grande. Geophys. Res. Lett.

Tian, Y., Zhou, Y., Sigloch, K., Nolet, G., Laske, G., 2011. Structure of North American mantle constrained by simultaneous inversion of multiple-frequency SH, SS, and Love waves. J. Geophys. Res. 116, B02307. http://dx.doi.org/10.1029/2010JB007704.

Van Wijk, J., Van Hunen, J., Goes, S., 2008. Small-scale convection during continental rifting: evidence from the Rio Grande Rift. Geology 36 (7), 575–578.

West, M., Gao, W., Grand, S., 2004a. A simple approach to the joint inversion of seismic body and surface waves applied to the southwest U.S. Geophys. Res. Lett. 31, L15615. http://dx.doi.org/10.1029/2004GL020373.

West, M., Ni, J., Baldridge, W.S., Wilson, D., Aster, R., Gao, W., Grand, S., 2004b. Crust and upper mantle shear wave structure of the southwest United States: implications for rifting and support for high elevation. J. Geophys. Res. 109, B03309. http://dx.doi.org/10.1029/2003JB00.

Wilson, D., 2003. Imagining crust and upper mantle seismic structure in the southwestern United States using teleseismic receiver functions. Lead. Edge 22, 232–237.

Wilson, D., Aster, R., 2005. Seismic imaging of the crust and upper mantle using regularized joint receiver functions, frequency–wave number filtering, and multimode Kirchhoff migration. J. Geophys. Res. 110, B05305. http://dx.doi.org/10.1029/2004JB00343.

Wilson, D., Aster, R., Ni, J., Grand, S., West, M., Gao, W., Baldridge, W.S., Semken, S., 2005a. Imaging the structure of the crust and upper mantle beneath the Great Plains, Rio Grande Rift, and Colorado Plateau using receiver functions. J. Geophys. Res. 110, B05306. http://dx.doi.org/10.1029/2004JB003492.

Wilson, D., Aster, R., West, M., Ni, J., Grand, S., Gao, Baldridge, W., Semken, S., Patel, P., 2005b. Lithospheric structure of the Rio Grande Rift. Nature 433, 851–854.

Wilson, D., Aster, R., Grand, S., Ni, J., Baldridge, W.S., 2010. High-resolution receiver function imaging reveals Colorado Plateau lithospheric architecture and mantle-supported topography. Geophys. Res. Lett. 37, L20313. http://dx.doi.org/10.1029/2010GL044799.

Woodward, L.A., 1977. Rate of crustal extension across Rio Grande Rift near Albuquerque, New Mexico. Geology 5, 269–272.

Xue, M., Allen, R.M., 2010. Mantle structure beneath the western United States and its implications for convection processes. J. Geophys. Res. 115, B07303. http://dx.doi.org/10.1029/2008JB006079.

Yang, Y., Ritzwoller, M.H., Lin, F.C., Moschetti, M.P., Shapiro, N.M., 2008. Structure of the crust and uppermost mantle beneath the western United States revealed by ambient noise and earthquake tomography. J. Geophys. Res. 113, B12310. http://dx.doi.org/10.1029/2008JB005833.

Yuan, H., Romanowicz, B., 2010. Lithospheric layering in the North American Craton. Nature 466, 1063–1068.

Yuan, H., Romanowicz, B., Fischer, K.M., Abt, D., 2011. 3-D shear wave radially and azimuthally anisotropic velocity model of the North American upper mantle. Geophys. J. Int. 184, 1237–1260.

Zhdanov, M.S., 2002. Geophysical Inverse Theory and Regularization Problems, Vol. 36. Elsevier.